

1  
2  
3  
4  
5  
6  
7  
8  
9  
10  
11  
12  
13  
14  
15  
16  
17  
18  
19  
20  
21

**Technique Note: Application of positive matrix factor analysis in  
heterogeneous kinetics studies utilizing the mixed-phase relative  
rates technique**

Y. Liu, S.-M. Li and J. Liggio\*

Air Quality Processes Research Section, Environment Canada, Toronto, M3H  
5T4, Canada

---

\*Corresponding author. Phone: 1-416-739-4840; fax: 1-416-739-4281;  
E-mail: [John.Liggio@ec.gc.ca](mailto:John.Liggio@ec.gc.ca)

22

23 **Abstract:**

24 The mixed-phase relative rate approach for determining aerosol particle organic  
25 heterogeneous reaction kinetics is often performed utilizing mass spectral tracers as a  
26 proxy for particle phase reactant concentration. However, sometimes this approach  
27 may be influenced by signal contamination from oxidation products during the  
28 experiment. In the current study, the mixed-phase relative rates technique has been  
29 improved by combining a Positive Matrix Factor (PMF) analysis with electron  
30 ionization Aerosol Mass Spectrometry (unit mass resolution), thereby removing the  
31 influence of  $m/z$  fragments from reaction products on the reactant signals. To  
32 demonstrate the advantages of this approach, the heterogeneous reaction between OH  
33 radicals and citric acid (CA) was investigated using a photochemical flow tube  
34 coupled to a compact time-of-flight aerosol mass spectrometer (C-ToF-AMS). The  
35 measured heterogeneous rate constant ( $k_2$ ) of citric acid toward OH was  
36  $(3.31 \pm 0.29) \times 10^{-12} \text{ cm}^3 \text{ molecule}^{-1} \text{ s}^{-1}$  at 298 K and  $(30 \pm 3) \% \text{ RH}$  and was several  
37 times greater than the results utilizing individual  $m/z$  fragments. This phenomenon  
38 was further evaluated for particulate-phase organophosphates (TPhP, TDCPP, and  
39 TEHP), leading to  $k_2$  values significantly larger than previously reported. The results  
40 suggest that heterogeneous kinetics can be significantly underestimated when the  
41 structure of the products is highly similar to the reactant and when a non-molecular  
42 tracer is measured with a unit mass resolution aerosol mass spectrometer. The results  
43 also suggest that the heterogeneous lifetime of organic aerosol in models can be

44 overestimated due to underestimated OH uptake coefficients. Finally, a comparison of  
45 reported rate constants implies that the heterogeneous oxidation of aerosols will be  
46 dependent upon a number of factors related to the reaction system, and that a single  
47 rate constant for one system cannot be universally applied under all conditions.

48

49

50

51

52

53

54

55

56

57

58

59

60

61

62

63

64

65

66

## 67 **1. Introduction**

68       Reaction kinetics data provide key parameters for both air quality and climate  
69 models. They are required to compute the trace gas and particle matter (PM) content  
70 of the atmosphere (Kolb et al., 2010) and to evaluate the atmospheric lifetime and fate  
71 for individual species. Organic particles make up 10-90 % of the global submicron  
72 particle mass in the lower troposphere (Zhang et al., 2011), and is comprised of  
73 various reactive organic species, which are subject to atmospheric heterogeneous  
74 oxidation. Previous studies have found that heterogeneous reactions with OH in  
75 particular, can lead to an increase in density, CCN activation (George and Abbatt,  
76 2010) and optical extinction (Cappa et al., 2011) of organic particulate matter.  
77 Therefore, there is a growing interest in understanding not only the mechanism of PM  
78 transformation through heterogeneous reactions including oxidation, but also  
79 determining the rates at which organic aerosols are chemically transformed in the  
80 atmosphere.

81       To this end, Donahue et al. (Donahue et al., 2005) and Hearn and Smith (Hearn  
82 and Smith, 2006) developed a mixed-phase relative rate technique for measuring  
83 organic PM component heterogeneous reaction kinetic rate constants. In this method,  
84 the rate constant of the compound of interest is determined from the decrease of its  
85 particle phase relative concentration as a function of oxidant exposure. The oxidant  
86 levels are simultaneously estimated via the measured loss of a gas phase reference  
87 compound after applying the known second-order rate constant ( $k_2$ ) toward the

88 oxidant. In this approach the rates of chemical change are given by,

89 
$$-\frac{dc_A}{dt} = k_{2,A}c_Ac_{Ox} \quad (1)$$

90 
$$-\frac{dc_R}{dt} = k_{2,R}c_Rc_{Ox} \quad (2)$$

91 where  $c_A$ ,  $c_R$  and  $c_{Ox}$  are the particle phase concentration of the compound of interest  
92 (A), the gas phase concentration of the reference compound (R) and oxidant  
93 (molecules  $\text{cm}^{-3}$ ) respectively, while  $k_{2,A}$  and  $k_{2,R}$  are the second-order rate constant of  
94 A and R to the oxidant ( $\text{cm}^3 \text{ molecule}^{-1} \text{ s}^{-1}$ ). A relative rate constant ( $k_r$ ) (ie: particle  
95 phase reaction rate of A, relative to the gas phase rate of R) can be derived by dividing  
96 Eq. (1) by Eq. (2). The derivation of  $k_r$  provides a means to obtain heterogeneous  
97 kinetic data without the need to know the absolute concentration of the oxidant. The  
98 differential and integral forms for the relative rates technique are shown as Eq. (3) and  
99 (4),

100 
$$\frac{dc_A}{c_A} = \frac{k_{2,A}}{k_{2,R}} \frac{dc_R}{c_R} = k_r \frac{dc_R}{c_R} \quad (3)$$

101 
$$\log \frac{c_A}{c_{A,0}} = k_r \log \frac{c_R}{c_{R,0}} \quad (4)$$

102 from which the relative rate constant ( $k_r$ ), is the slope of the line derived by plotting  
103 the logarithmic relative concentration of A against that of R (relative to initial  
104 conditions;  $c_{A,0}$ ). The second-order heterogeneous rate constant of the compound of  
105 interest ( $k_{2,A}$ ) towards the oxidant may then be calculated using the obtained  $k_r$  and the  
106 known  $k_{2,R}$  (ie:  $k_{2,A} = k_r \times k_{2,R}$ ).

107 Using this method, a number of studies have quantified the uptake coefficients of  
108  $\text{O}_3$ , OH, Cl, and  $\text{NO}_3$  on various organic particles, and the corresponding second order  
109 rate constants for the degradation of organic compounds (Hearn and Smith,

110 2006;George et al., 2007;Lambe et al., 2007;McNeill et al., 2007;McNeill et al.,  
111 2008;Smith et al., 2009;Kessler et al., 2010;Renbaum and Smith, 2011;Kessler et al.,  
112 2012;Liu et al., 2012;Sareen et al., 2013).

113 Although gas chromatograph mass spectrometry (GC-MS) has been widely used  
114 in the kinetics studies (Weitkamp et al., 2008a;Weitkamp et al., 2008b;Lambe et al.,  
115 2009;Isaacman et al., 2012), quantifying the particle phase loss of an organic  
116 compound in such studies often relies upon aerosol mass spectrometry techniques to  
117 monitor specific particle phase reactant ions of interest in semi-real time. Aerosol  
118 mass spectrometry instruments utilizing high resolution detection and soft ionization  
119 techniques, such as chemical ionization (Aerosol CIMS) (Hearn and Smith,  
120 2006;McNeill et al., 2007;McNeill et al., 2008;Renbaum and Smith, 2011;Sareen et  
121 al., 2013) and vacuum ultraviolet photo-ionization (VUV-ATOFMS)(Liu et al., 2012),  
122 have been utilized to measure the concentration of the target organic compounds in  
123 particles. However, Aerosol Time-of-Flight or Quadrupole Mass Spectrometry  
124 (ToF-AMS or Q-AMS) employing electronic ionization (EI; 70 eV) as an ion source  
125 remains the prevalent instrument used in such organic particle experiments. In  
126 utilizing this approach, a specific fragment (usually the fastest-decaying ions in the  
127 spectrum) is often chosen as a tracer for the particle phase compound of interest. For  
128 example,  $m/z$  297 has been selected as a tracer for bis(2-ethylhexyl) sebacate (BES)  
129 (George et al., 2007),  $m/z$  71 for hexacosane (Lambe et al., 2007),  $m/z$  113 for  
130 squalane (Smith et al., 2009),  $m/z$  104 and 144 for erythritol and levoglucosan  
131 (Kessler et al., 2010), and  $m/z$  152, 68 and 98 for 1,2,3,4-butanetetracarboxylic acid,

132 citric acid and tartaric acid (Kessler et al., 2012) respectively.

133       However, the use of EI in conjunction with a particle vaporizer in the AMS  
134 results in heavy fragmentation for organic compounds due to the high energy  
135 associated with the EI source (70 eV) and the high temperature (~873 K) of the  
136 vaporizer (Jayne et al., 2000; Allan et al., 2003). Under such conditions, the tracer m/z  
137 fragment is prone to interferences due to (1) the fragmentation of larger ions and/or  
138 molecules and (2) fragments from particle phase oxidation products. Both can  
139 contribute to the tracer m/z signal, sometimes leading to an insensitive or nonlinear  
140 response of the tracer m/z to the concentration of the target reactant during oxidation.  
141 The same may also be true for the m/z for the molecular ion should one exist. In  
142 particular, it is true if the structure of the product is highly similar to the reactant and  
143 when the tracer is measured with a unit-mass resolution (UMR) aerosol mass  
144 spectrometer. Although it is often assumed that the chosen tracer ion does not  
145 contribute significantly to the mass spectra of any possible oxidation products or vice  
146 versa (Kessler et al., 2010), this is not always the case. In our previous work, we  
147 observed that the magnitude of the second order heterogeneous rate constant ( $k_2$ )  
148 increases as a function of increasing m/z of the fragment chosen as a tracer of the  
149 parent molecule (Liu et al., 2014). The same trend has also been observed for the OH  
150 oxidation of ambient biogenic secondary organic aerosol (SOA) (Slowik et al., 2012).  
151 This suggests an interference from the fragments selected, and points to the necessity  
152 to separate the signals of the compound of interest, from other compounds (products  
153 and/or fragment) for kinetic studies.

154 In the current study, we improve the mixed-phase relative rate technique used for  
155 studies of the heterogeneous oxidation of organic aerosol (OA) using positive matrix  
156 factorization (PMF) analysis of UMR-AMS derived kinetic data. Heterogeneous  
157 kinetics of citric acid (CA) toward OH oxidation was studied in a photo-chemical  
158 flow tube coupled to an Aerodyne C-ToF-AMS and an Ionicon Analytik High  
159 Resolution Proton Transfer Reaction Mass Spectrometer (PTR-ToF-MS). As it was  
160 applied to heterogeneous oxidation of ambient biogenic SOA (Slowik et al., 2012),  
161 PMF analysis was used to successfully deconvolve the full mass spectra of the  
162 reactant from the potential oxidation products, hence allowing proper accounting of  
163 the time evolution of reactant concentrations during photochemical oxidation.

## 164 **2. EXPERIMENTAL DETAILS**

165 **2.1 Flow tube experiments.** A detailed schematic representation of the experimental  
166 system utilized in this study has been described elsewhere (Liu et al., 2014). Briefly,  
167 organic particles (citric acid) were generated via atomization (model 3706, TSI), dried  
168 through a diffusion drier and size-selected with a differential mobility analyzer (DMA)  
169 (model 3081, TSI). The dried, monodispersed CA particles were introduced into the  
170 flow tube reactor and exposed to differing OH concentrations. OH radicals were  
171 produced by the photolysis of O<sub>3</sub> at 254 nm in the presence of water vapor. O<sub>3</sub> was  
172 generated by passing zero air through an O<sub>3</sub> generator (OG-1, PCI Ozone Corp.). The  
173 O<sub>3</sub> concentration in the reactor was measured using an O<sub>3</sub> monitor (model 205, 2B  
174 Technologies) and ranged from 0-1000 ppbv. Relative humidity (RH) in the reactor  
175 was held constant (30±3) % by varying the ratio of wet to dry air used as an air source,



176 and was measured at the exit of the flow tube reactor. The temperature was held  
177 constant at 298 K by circulating a temperature controlled fluid through the outer  
178 jacket of the reactor. The residence time in the flow reactor was 52 s. The steady-state  
179 OH exposures were varied from 0 to  $\sim 7.0 \times 10^{11}$  molecules  $\text{cm}^{-3}$  s which was estimated  
180 on the basis of the decay of methanol from (as a reference compound) its reaction  
181 with OH. The decay of methanol from its reaction with OH was measured using the  
182 PTR-ToF-MS. The  $k_2$  of methanol,  $9.4 \times 10^{-13}$   $\text{cm}^3$  molecule $^{-1}$  s $^{-1}$ , was used for the OH  
183 exposure calculation (Atkinson and Arey, 2003).

184 OH radical reactions were performed in a custom-made reactor consisting of two  
185 electro-polished stainless steel cylinders with inner diameter of 7.3 cm. The first stage  
186 contained static mixing elements (StaMixCo) to ensure that particles and gas phase  
187 species were well mixed prior to entering the reaction region (second stage). Fluid  
188 dynamics simulations of the flow tube confirmed that particles and gas phase species  
189 were well mixed in the reactor, with a uniform initial velocity profile. The size and  
190 composition of the particles exiting the reactor were measured by a scanning mobility  
191 particle sizer (SMPS, TSI) and an Aerodyne C-ToF-AMS (Drewnick et al., 2005)

192 Control experiments demonstrated that O<sub>3</sub> or 254 nm light exposure did not lead  
193 to the decomposition of CA. Analytic grade CA (EM, Germany) was used as received.  
194 18.2 MΩ water was used as solvent.

## 195 **2.2 PMF analysis and kinetics calculation.**

196 PMF is a multivariate factor analysis tool that decomposes a matrix of speciated  
197 sample data into two matrices, namely, factor contributions and factor profiles

198 (Paatero and Tapper, 1994), such that

$$199 \quad x_{ij} = \sum_p g_{ip} f_{pj} + e_{ij} \quad (5)$$

200 Where  $i$  and  $j$  refer to row and column indices in the matrix, respectively,  $p$  is the  
201 number of factors in the solution,  $x_{ij}$  is an element of the  $m \times n$  matrix  $X$  of measured  
202 data elements to be fit, and  $e_{ij}$  is the residual. Results are constrained so that no  
203 sample can have a negative source contribution. The PMF solution minimizes the  
204 object function  $Q$  (Eq.6), based upon the uncertainties ( $u$ ) (Norris and Vedantham,  
205 2008).

$$206 \quad Q = \sum_{i=1}^n \sum_{j=1}^m \left( \frac{e_{ij}}{u_{ij}} \right)^2 \quad (6)$$

207 Its ability to separate the signals of a multi-component matrix has been well  
208 established. PMF analysis has been widely used for source apportionment of ambient  
209 particles in field measurements (Song et al., 2006; Yuan et al., 2006; Viana et al.,  
210 2008; Ulbrich et al., 2009; Liggio et al., 2010; Schwartz et al., 2010). Three secondary  
211 organic aerosol factors (SOA1, SOA2, SOA3) have been identified for OH initiated  
212 oxidation of laboratory SOA (George and Abbatt, 2010). Similarly, SOA factors have  
213 also been successfully isolated in OH oxidation of ambient biogenic SOA (Slowik et  
214 al., 2012). Therefore, the use of PMF for separating the reactants from the products in  
215 laboratory studies aimed at using the relative rates method for heterogeneous kinetic  
216 studies would seem to be a reasonable approach.

217 The AMS data for CA oxidation from all experiments combined were used as  
218 input into the PMF Evaluation Toolkit (PET) v2.05 (Paatero, 1997; Paatero and Tapper,  
219 1994; Ulbrich et al., 2009) to separate the signals of CA and the corresponding

220 oxidation products. In the AMS data, the  $m$  rows of  $X$  are ensemble average mass  
221 spectra (MS) of typically tens of thousands of particles measured over each averaging  
222 period (typically 2 min) and the  $n$  columns of  $X$  are the time series (TS) of each  $m/z$   
223 sampled.

224 PMF analyses were done in the robust mode. The default convergence criteria  
225 were not modified. The  $Q$  values as a function of FPEAK from -1 to +1 were  
226 examined (Reff et al., 2007). For the variables with signal-to-noise ratio (SNR) less  
227 than 0.2 (“bad” variables) and downweight variables with SNR between 0.2 and 2  
228 (“weak” variables), their error estimates were increased by a factor of 10 and 3,  
229 respectively, as recommended by Paatero and Hopke (Paatero and Hopke, 2003). In  
230 this study, the SNR of all  $m/z$  fragments are larger than 0.2. The error values for  $m/z$   
231 44, 18, 17 and 16 were multiplied by  $\sqrt{4}$ .

232 The extracted factor profiles (mass spectra for CA and the oxidation products)  
233 were compared with the NIST mass spectrum of pure CA and that measured with the  
234 C-ToF-AMS directly via atomization. The temporal concentration profiles (factor  
235 contributions) of CA were further confirmed via comparison to the known  
236 experimental conditions used for kinetics calculations (ie: zero OH exposure should  
237 result in a CA factor contribution of 100 %). For comparison with the PMF results,  
238 the kinetic rate constants ( $k_r$ ) were also calculated using specific individual tracers of  
239 CA at  $m/z$  87, 129 and 147, separately. The  $k_r$  of CA toward methanol was calculated  
240 according to Eq. (4). The  $k_2$  of CA was further calculated with the known  $k_2$  of  
241 methanol and  $k_r$ .

242 The reactive uptake coefficient of OH ( $\gamma_{\text{OH}}$ ) with CA was calculated using the  
243 following formulation (Kessler et al., 2010; Worsnop et al., 2002; Kessler et al.,  
244 2012; Liu et al., 2012):

$$245 \gamma_{\text{OH}} = \frac{2D_p \rho_{\text{CA}} N_A}{3v_{\text{OH}} M_{\text{CA}}} \varphi k_2 \quad \text{Eq (7)}$$

246 Where  $D_p$  is the surface-weight average particle diameter of unreacted particles (cm),  
247  $\rho_{\text{CA}}$  is the density of CA ( $\text{g cm}^{-3}$ ),  $N_A$  is Avogadro's number,  $v_{\text{OH}}$  is the average speed  
248 of OH radicals in the gas phase ( $\text{cm s}^{-1}$ ),  $M_{\text{CA}}$  is the molecular weight of CA ( $\text{g mol}^{-1}$ ),  
249  $\varphi$  is a correction factor for diffusion of OH from the gas phase to particle phase.

250

## 251 **3.0 Results**

### 252 **3.1 PMF analysis of AMS data.**

253 To ensure that oxidation of CA in particles does not result in a PTR-ToF-MS  
254 response for methanol in the gas phase (thus compromising the OH radical reference  
255 measurement), the oxidation of pure CA was performed in the absence of methanol,  
256 with no gas phase methanol signal detected by the PTR-ToF-MS. The mass  
257 concentration of the OA measured with the AMS during oxidation is shown in Figure  
258 1A, which was constant. The results of Figure 1A demonstrate that the aerosol source  
259 is adequately stable for kinetic studies to be performed.

260 A two factor solution from the PMF analysis accounts for 99.98 % of the  
261 variance of the data. When the number of factors is greater than 2, none of the  
262 obtained factors resembles that of pure CA, whose contribution should be  
263 approximately 100 % when OH is absent in the reactor. Figures 1B and C represent

264 the temporal variations of the typical 2-factor PMF solution of AMS data when CA is  
265 exposed to varying OH concentrations. The error bars indicate the rotational  
266 uncertainty in the PMF analysis. Three independent experiments were performed to  
267 test the response of CA signal to OH exposure (determined by O<sub>3</sub> concentration). In  
268 the first and the third experiments, OH exposure was stepped downwards (high to low  
269 OH) by changing the power of O<sub>3</sub>-generator with the same flow rate and RH, while  
270 the inverse sequence was performed in the second experiment.

271 As demonstrated in Figure 1B and C, in the absence of OH radical (labeled“0”),  
272 factor 1 (Figure 1B) accounts for (94.7±0.9) % of the OA mass, while factor 2 (Figure  
273 1C) contributes (6.2±0.7) % of OA. This is consistent with the experimental  
274 conditions of zero OH radical (ie: no oxidation), and suggests that factor 1 should be  
275 assigned to the citric acid reactant. Impurities in the CA or the water used to atomize  
276 CA likely contributed to factor 2. When OH exposure was decreased in a step-wise  
277 manner in the first and the third experiment (Figure 1B), the extracted factor  
278 representative of CA (factor 1) increased synchronously, and is accompanied with a  
279 decrease in factor 2. Therefore, factor 2 is interpreted as the OH oxidation products of  
280 CA. This is consistent with the second experiment, where the inverse trend was  
281 observed with a step-wise OH exposure increase. Based upon this evidence, we  
282 conclude that changes in the time series of factors 1 and 2 extracted by PMF are  
283 consistent with the expected response to OH exposures, namely, that higher OH  
284 exposure resulted in a decrease in CA (factor 1) and an increase in the oxidation  
285 products (factor 2).

286 The factor profiles (ie: mass spectra) extracted by PMF analysis are shown in  
287 Figure 2. The main fragments of CA including m/z values 129 ( $C_5H_5O_4^+$ ) and 87  
288 ( $C_3H_3O_3^+$ ) are present in factor 1 (Figure 2A). These fragments are in good agreement  
289 with the NIST mass spectra of pure CA and the mass spectrum of pure CA particles  
290 measured with the C-ToF-AMS (Figure 3). Figure 4 further compared the normalized  
291 mass spectra of factor 1 and pure CA directly measured with the C-ToF-AMS. The  
292 relative intensities for all ions of pure CA are linearly correlated with that of factor 1  
293 with a slope of 0.985 and R of 0.9999. This further confirmed that factor 1 should be  
294 assigned to unreacted CA. Figure 2C shows the difference mass spectra (factor 2 –  
295 factor 1). Consumption of m/z values 147 ( $C_5H_7O_5^+$ ), 129, 87, 85 ( $C_4H_5O_2^+$ ) and 60  
296 ( $C_2H_4O_2^+$ ) can be observed, which is consistent with the assignment that factor 2  
297 belongs to oxidation products of CA. However, small changes in the relative  
298 intensities of these peaks suggest that the structure of the oxidation products of CA are  
299 likely similar to that of CA. For example, as shown in Figure 2A and B, the intensity  
300 of m/z 129 and 87 in factor 2 are  $0.0125 \pm 0.0046$  and  $0.0218 \pm 0.0013$  compared to  
301  $0.0141 \pm 0.0046$  and  $0.0235 \pm 0.0013$  in factor 1.

302 The changes of the relative concentrations of gas phase methanol and particle  
303 phase CA are shown in Figure 5. The signal of CA extracted by PMF analysis also  
304 responded to OH exposure as expected, when methanol was present in the gas phase,  
305 which is similar to that of Figure 1. The relative intensities of the typical tracers of CA  
306 at m/z 87, 129 and 147 are shown in Figure 5C. As shown in Figure 5 B and C, the  
307 drop in the PMF product factor is substantially greater than that of any of the

308 individual ions. In addition, the consumption of the smaller tracer ( $m/z$  87) is  
309 substantially lower than that of the larger ones ( $m/z$  values 129 and 147). For example,  
310 the maximum consumption of CA extracted with PMF analysis is approximately 80 %,  
311 in comparison to ~30 %, ~10 % and 5 % for  $m/z$  values 147, 129 and 87, respectively.  
312 These results support the small differences in the mass spectra between the unreacted  
313 CA and its oxidation products as shown in Figure 2. Furthermore, it suggests that the  
314 measured loss of these fragments, which were supposedly only derived from CA, had  
315 in fact contributions from the fragmentation of the products of CA oxidation. This  
316 ultimately would lead to an underestimation of the second order heterogeneous rate  
317 constant (or OH uptake coefficients) if these fragments were chosen as the proxies for  
318 the particle phase concentration of CA. In particular, the difference between the  
319 PMF-factor decay rate and the marker-ion decay rate is mathematically possible only  
320 when the two factors (reactants and products) are extremely similar.

321 **3.2 Reaction kinetics.** The saturation vapor pressure of CA at 298K is  $1.6 \times 10^{-7}$  Pa  
322 (Huisman et al., 2013), thus 99.9% of CA should be present in the particle phase  
323 under the current experimental conditions according to a partition model (Kroll and  
324 Seinfeld, 2008; Pankow, 1994). Although new particle formation was observed with a  
325 CPC in the experiments (at the exit of the reactor), it has no influence on the measured  
326 mass concentration of OA due to the small particle size of the new particles. This is  
327 well supported by the constant mass concentration of OA measured with the AMS  
328 during oxidation experiments (Figure 1A). In addition, as pointed out in our previous  
329 work (Liu et al., 2014), evaporation of CA from particles could potentially contribute

330 to the decreases in particle phase CA concentration observed as a function of OH  
331 exposure. If CA evaporation was at play, the derived reaction rates will be  
332 overestimated using either the present approach or the simpler methods of using  
333 single fragments. The evaporation of CA from the particle phase under these  
334 experimental conditions from control experiments is less than 0.005 % based upon an  
335 evaporation model (Jacobson, 2005). This implies that the observed changes in CA  
336 concentration in the particle phase were due to the particle phase reaction.

337 The relative rates (relative to initial conditions) for CA and methanol in these  
338 experiments are shown in Figure 6. The logarithmic  $c/c_0$  of CA both measured with  
339 the tracers and extracted with PMF analysis linearly correlated to that of methanol  
340 with  $R^2 > 0.95$ . The derived relative rate constant based upon PMF analysis is  
341  $3.01 \pm 0.27$ , while it is  $0.72 \pm 0.05$  and  $0.22 \pm 0.01$  for  $m/z$  values 147 and 129,  
342 respectively. Applying the  $k_2$  value of methanol towards OH of  $9.4 \times 10^{-13} \text{ cm}^3$   
343  $\text{molecule}^{-1} \text{ s}^{-1}$  at 298 K (Atkinson and Arey, 2003), the  $k_2$  of CA is calculated as  
344  $(2.83 \pm 0.25) \times 10^{-12}$  using the PMF approach, or  $(6.77 \pm 0.47) \times 10^{-13}$  using the single  
345 tracer at  $m/z$  147 and  $(2.02 \pm 0.01) \times 10^{-13} \text{ cm}^3 \text{ molecule}^{-1} \text{ s}^{-1}$  using the single tracer at  
346  $m/z$  129, respectively. The reaction between methanol and OH radicals occurs in the  
347 gas phase, while for the CA oxidation it occurs in particle phase. Thus it is necessary  
348 to correct for OH diffusion from the bulk gas phase to the particle phase. Applying a  
349 diffusion correction utilizing a previously developed empirical formula (Fuchs and  
350 Sutugin, 1970; Worsnop et al., 2002; Widmann and Davis, 1997), the  
351 diffusion-corrected  $k_2$  is  $(3.31 \pm 0.29) \times 10^{-12}$  using the PMF approach, and



352  $(7.92\pm 0.55)\times 10^{-13}$  and  $(2.36\pm 0.01)\times 10^{-13}$   $\text{cm}^3 \text{ molecule}^{-1} \text{ s}^{-1}$  using single tracers at m/z  
353 147 and 129, respectively. The diffusion-corrected  $\gamma_{\text{OH}}$  is calculated as  $2.74\pm 0.24$   
354 using the PMF approach, and  $0.66\pm 0.05$  and  $0.20\pm 0.01$  using single tracers at m/z 147  
355 and 129, respectively. The  $\gamma_{\text{OH}}$  for a number of different organic particles have  
356 previously been measured, and are in the range of 0.3 – 2.0 (Kessler et al.,  
357 2010; George et al., 2007; Hearn and Smith, 2006; Lambe et al., 2007; Smith et al.,  
358 2009; Kessler et al., 2012). As pointed out by Hearn and Smith (2006), the large  $\gamma$   
359 implies that secondary radical reactions within the particles could play a significant  
360 role in heterogeneous chemistry, particularly since gaseous citric acid in these studies  
361 is insignificant.

362 It should be pointed out that oxidant diffusion in the particle phase should lead to  
363 a concentration gradient of oxidant and a negative impact on reaction kinetics  
364 (Donahue et al., 2005). However, as shown in Figure 6, this effect is negligible under  
365 the current experimental conditions. Based upon the measured  $c/c_0$  and the initial  
366 diameter of the CA particles, the maximum OH diffusion depth is approximately 25  
367 nm. Given the residence time ( $\tau$ ) in this study (52 s), a significant OH concentration  
368 gradient will exist in particle phase if the  $D_{\text{OH}}$  in CA particles is smaller than  $1.2\times 10^{-17}$   
369  $\text{m}^2 \text{ s}^{-1}$  ( $D=l^2/\tau$ ) (Donahue et al., 2005). At the present time, the  $D_{\text{OH}}$  in CA particles is  
370 unavailable. However, Price et al. (Price et al., 2014) have reported the diffusion of  
371  $\text{D}_2\text{O}$  in several organics (sucrose and levoglucosan) to be larger than  $\sim 1\times 10^{-16} \text{ m}^2 \text{ s}^{-1}$   
372 even under dry condition. This implies that a gradient in OH concentration in the CA  
373 particles is negligible under the current conditions.

374 **4. Discussion**

375 Kessler et al. (Kessler et al., 2012) have reported the  $k_2$  of CA toward OH to be  
376  $(4.3\pm 0.8)\times 10^{-13}$  cm<sup>3</sup> molecule s<sup>-1</sup> at 308 K and 30 % RH with an Aerodyne HR-AMS.  
377 In their work, the diameter of particles and RH were equivalent to the current work,  
378 while their experimental temperature was 10 K higher. In addition, a m/z fragment of  
379 68 was used as a tracer for CA in their work to derive the heterogeneous rate constant.  
380 Conversely, no significant consumption of m/z 68 was observed in the current study.  
381 The lack of a m/z 68 fragment consumption here may be explained by the choice of  
382 reaction conditions. In the work of Kessler et al., OH concentration exposure  
383  $(0\sim 7\times 10^{12}$  molecule cm<sup>-3</sup> s) was approximately an order of magnitude higher than that  
384 reported here. Recent evidence suggests that the product distribution during OA  
385 oxidation greatly depends upon OH exposure levels (Wilson et al., 2012). Hence, it is  
386 possible that more oxidized products formed via multi-generational chemistry at high  
387 OH were formed, which may have less of an influence on the signal of the chosen  
388 tracer (m/z 68), and result in product AMS spectra which are significantly different  
389 than that of the reactant thus mitigating the use of PMF (which was not the case here).  
390 In studies of the OH oxidation of squalane (Sq) (Smith et al., 2009; Wilson et al.,  
391 2012), the first generation product (SqO) was the primary contributor to the products  
392 when the OH exposure was the same as the highest OH level in the current study  
393  $(7.0\times 10^{11}$  molecules cm<sup>-3</sup> s), while higher generation products were predominant at  
394 OH exposures was greater than  $\sim 2\times 10^{12}$  molecules cm<sup>-3</sup> s. Although not directly  
395 comparable, it is reasonable to assume that lower OH exposure in the current work

396 should lead primarily to the first generation products, which are highly similar to CA.  
397 However, the formation of multi-generation products cannot be completely ruled out.  
398 Secondly, the difference in OA and oxidant concentrations as well as timescale may  
399 also have an influence on the product distribution. Thirdly, a high resolution  
400 time-of-flight aerosol mass spectrometer (HR-ToF-AMS) was used in their work,  
401 while a C-ToF-AMS with unit-mass resolution was used in this study. The higher  
402 mass resolution of the HR-ToF-AMS relative to a C-ToF-AMS, may further reduce  
403 the influence of product fragments on  $m/z$  68 (or others). Finally, differences in  
404 temperature or other reaction conditions between experiments may also have led to  
405 differences in the morphology of CA and subsequent differences in the reactivity of  
406 CA.

407       Given the above discrepancy in the consumption of  $m/z$  68, the fragments at  $m/z$   
408 129 and 147 were used as tracers in this work. The measured  $k_2$  of CA utilizing  $m/z$   
409 129 and 147 in this study is of the same order of magnitude as that reported in Kessler  
410 et al. (2012). However, as shown in Figure 3C, the consumption of  $m/z$  87 is much  
411 lower than that of  $m/z$  129. The apparent  $k_2$  of CA based on  $m/z$  87 is  $(9.9\pm 0.8)\times 10^{-14}$   
412  $\text{cm}^3 \text{ molecule}^{-1} \text{ s}^{-1}$ , and the diffusion-corrected  $k_2$  is  $(1.16\pm 0.09)\times 10^{-13} \text{ cm}^3 \text{ molecule}^{-1}$   
413  $\text{s}^{-1}$ . This suggests that the derived rate constant greatly depends upon the size of the  
414 tracer fragment, with larger fragments resulting in larger values of  $k_2$  in this study.  
415 This is consistent with previous work investigating the OH oxidation of tris-phenyl  
416 phosphate (TPhP) (Liu et al., 2014) and ambient biogenic SOA (Slowik et al., 2012).  
417 The  $k_2$  of CA based upon PMF analysis is approximately an order of magnitude larger

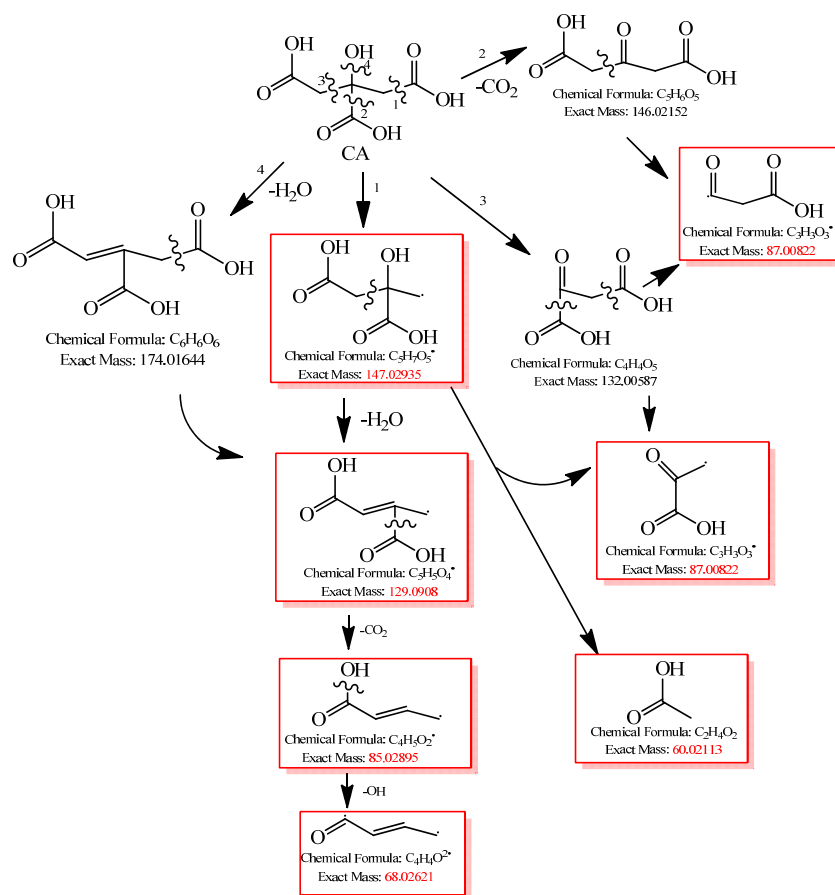
418 than the Kessler result measured with the tracer at  $m/z$  68, and 4.2 times greater than  
419 that calculated based upon  $m/z$  147 in this study. The differences in product  
420 distributions that may arise between this and the work of Kessler et al., consistent  
421 with the fact that  $m/z$  68 is not consumed in the current study, suggests that the PMF  
422 approach was likely required in this work to separate similar product and reactant  
423 spectra ultimately caused by lower OH exposure.

424 A number of factors may be responsible for the discrepancy between derived rate  
425 constants. It has previously been observed that the presence of  $O_3$  can inhibit the rate  
426 of OH reaction, perhaps by reacting with OH radicals or by  $O_3$  or intermediate species  
427 blocking surface active sites (Renbaum and Smith, 2011). A Langmuir-Hinshelwood  
428 mechanism has been observed for the reaction of  $O_3$  on organic surfaces (Pöschl,  
429 2005). It has also been demonstrated that a higher concentration of gas phase reactant  
430 often leads to a lower uptake coefficient due to surface saturation (Ma et al., 2010 ;Li  
431 et al., 2002). Differences in  $k_2$  may also arise from the competition between reaction  
432 products and reactants for available OH, or via the blocking or coating of the reactant  
433 by products which would require liquid phase diffusion of OH to degrade the original  
434 CA. In experiments with higher OH exposures (Kessler et al 2012) it is possible that  
435 significantly more product mass is mixed and/or coated onto the original particle thus  
436 decreasing the perceived  $k_2$ . Different timescales and concentrations of reactants  
437 might also lead to different rate constants (Che et al., 2009). Finally, as pointed out  
438 above, the differing reaction conditions may have led to a different CA morphology  
439 and subsequent differences in the reactivity towards OH. The significant difference

440 between the reported rate constants highlights an important issue in heterogeneous  
441 reactions of the atmosphere, and in the experiments trying to derive such kinetics. It  
442 implies that the particle composition and/or morphology as determined by the reaction  
443 conditions in the laboratory or the ambient atmosphere will have a large effect on the  
444 OH kinetics.

445 Citric acid is a hydroxyl substituted poly carboxyl acid. Scheme 1 summarizes its  
446 possible fragmentation pathways. The typical mass peaks including  $m/z$  147, 129, 87,  
447 85 and 68 would result from this scheme and were indeed observed. The fragments at  
448  $m/z$  129, 87, 85 and 68 are also likely from CA oxidation products fragments, and  
449 hence their signal intensities may be highly influenced by products and/or larger  
450 fragments, in particular, when the oxidized products are highly similar to the reactant.  
451 In some instances, oxidation products can exhibit similar fragmentation pathways as  
452 the reactants. This is likely the case for the smaller fragments of CA. For example,  
453 scheme 2 illustrates the possible fragmentation pathways of  
454 2,3-dihydroxypropane-1,2,3-tricarboxylic acid, which is one of the possible products  
455 from the OH oxidation of citric acid in terms of the general chemistry described by  
456 Atkinson et al. (Atkinson, 1986). As observed in Scheme 2, there are several pathways  
457 leading to the fragment at  $m/z$  87, implying that the decrease in the signal of  $m/z$  87  
458 due to CA oxidation is likely to be compensated by fragments from the oxidation  
459 products. In addition, it is also possible to form fragments with the same  $m/z$  as the  
460 parent citric acid if the dehydration reaction (the 6<sup>th</sup> path in Scheme 2) takes place  
461 initially. Other possible reaction products might also play similar roles in the

462 fragments. This is highly possible when the product distribution contains products  
463 which are structurally similar to the reactant under low oxidant exposure conditions.



464

465

Scheme 1. Possible fragmentation pathways for citric acid.

466



479 435), respectively. The typical evolution of the PMF factors of TPhP, TDCPP, and  
480 TEHP are shown in Figures S1-3. For TPhP, the measured  $k_2$  values derived by both  
481 methods are comparable within the experimental uncertainties, while  $k_2$  of TDCPP  
482 and TEHP based upon PMF analysis is 1.5 and 1.6 times larger than that using the  
483 chosen tracers. The good agreement between methods for TPhP is likely due to the  
484 fact that the molecular ion peak ( $M^+$ ) is measurable for TPhP with the AMS, while it  
485 is not observable for TDCPP, TEHP and CA. Therefore, the influence of secondary  
486 fragmentation from larger fragments has little influence on the signal of  $M^+$  for TPhP.  
487 These results also demonstrate that a substantial underestimation of rate constants  
488 could result when a non-molecular ion tracer is used to monitor the particle phase  
489 concentration of organic matter with UMR-AMS for heterogeneous kinetic studies.  
490 The discrepancy between the tracer and PMF based methods for other compounds  
491 will depend upon a number of factors including: structure of products, OH exposure  
492 level, particle morphology, and organic species competing OH reactions.

493

## 494 **5.0 Implications and Conclusions**

495 The measured  $k_2$  for citric acid toward OH is  $(3.31 \pm 0.29) \times 10^{-12} \text{ cm}^3 \text{ molecule}^{-1}$   
496  $\text{s}^{-1}$  at 298 K and 30 % RH. This value is at least 4.2 times greater than that calculated  
497 on the basis of atypical tracer  $m/z$  147. Although the tracer and PMF approaches can  
498 at times agree (Kroll, 2014) and the tracer and molecular-ion approaches can  
499 sometimes agree as well (Smith et al., 2009), our results suggest that the  
500 heterogeneous kinetics of OA is underestimated when a non-molecular ion peak is



501 used as the tracer to measure the particle phase concentration of OA based on  
502 UMR-AMS. In model simulations, the reactive uptake coefficient of OH or other  
503 radicals, which are calculated based upon  $k_2$ , is an important parameter in evaluating  
504 the fate of OA during transport. The current results suggest that the lifetime of OA  
505 estimated in models due to heterogeneous oxidation might be overestimated for a  
506 reaction system where the products are highly similar to the reactant and the kinetic  
507 data are derived by individual non-molecular m/z tracers of OA. The results also  
508 suggest that it may be necessary to revisit the kinetic data of other organic aerosol  
509 components (and OH uptake coefficients) which have been derived using the relative  
510 rates technique (George et al., 2007; Lambe et al., 2007) based on UMR-AMS. Finally,  
511 these results imply that the heterogeneous oxidation of aerosols will be dependent  
512 upon a number of factors related to the reaction system, and that a single rate constant  
513 for one system cannot be universally applied under all conditions. Future work is thus  
514 required to elucidate the chemical and physical parameters which control the OH  
515 heterogeneous reaction kinetics and the associated need to apply PMF for a variety of  
516 chemical systems. This may be best accomplished through systematic application of  
517 the PMF approach to species with differing mass spectral characteristics, such as  
518 linear/branched alkanes, monocarboxylic acids and other oxygenates. As illustrated in  
519 this study, the kinetics derived with PMF may differ from that derived with tracer ions,  
520 with both based upon EI-AMS approaches. This highlights the usefulness of  
521 measurements from CIMS, GC-MS and VUV-AMS, for the determination of  
522 heterogeneous loss rates, since these instruments are more likely to retain the reactant

523 molecular information.

524

## 525 **Supporting Information**

526 Supplementary material related to this article is available online at:

527

## 528 **Acknowledgements**

529 This research was funded by the Chemicals Management Plan (CMP) and the Clean

530 Air Regulatory Agenda (CARA).

## 531 **Literature Cited:**

532 Allan, J. D., Jimenez, J. L., Williams, P. I., Alfarra, M. R., Bower, K. N., Jayne, J. T., Coe, H., and  
533 Worsnop, D. R.: Quantitative sampling using an Aerodyne aerosol mass spectrometer 1. Techniques of  
534 data interpretation and error analysis, *J. Geophys. Res.*, 108, 4090, 10.1029/2002jd002358, 2003.

535 Atkinson, R.: Kinetics and Mechanisms of the Gas-Phase Reactions of the Hydroxyl Radical with  
536 Organic Compounds under Atmospheric Conditions, *Chem. Rev.*, 85, 69-201, 1986.

537 Atkinson, R., and Arey, J.: Atmospheric Degradation of Volatile Organic Compounds, *Chem. Rev.*, 103,  
538 4605-4638, 2003.

539 Cappa, C. D., Che, D. L., Kessler, S. H., Kroll, J. H., and Wilson, K. R.: Variations in organic aerosol  
540 optical and hygroscopic properties upon heterogeneous OH oxidation, *J. Geophys. Res.*, 116, D15204,  
541 10.1029/2011jd015918, 2011.

542 Che, D. L., Smith, J. D., Leone, S. R., Ahmed, M., and Wilson, K. R.: Quantifying the reactive uptake  
543 of OH by organic aerosols in a continuous flow stirred tank reactor, *Phys. Chem. Chem. Phys.*, 11,  
544 7885-7895, 10.1039/b904418c, 2009.

545 Donahue, N. M., Robinson, A. L., Hartz, K. E. H., Sage, A. M., and Weitkamp, E. A.: Competitive  
546 oxidation in atmospheric aerosols: The case for relative kinetics, *Geophys. Res. Lett.*, 32, L16805,  
547 10.1029/2005gl022893, 2005.

548 Drewnick, F., Hings, S. S., DeCarlo, P., Jayne, J. T., Gonin, M., Fuhrer, K., Weimer, S., Jimenez, J. L.,  
549 Demerjian, K. L., Borrmann, S., and Worsnop, D. R.: A New Time-of-Flight Aerosol Mass  
550 Spectrometer (TOF-AMS)—Instrument Description and First Field Deployment, *Aerosol Sci. Technol.*,  
551 39, 637-658, 2005.

552 Fuchs, N. A., and Sutugin, A. G.: *Highly Dispersed Aerosols*, Butterworth-Heinemann, Newton, MA,  
553 1970.

554 George, I. J., Vlasenko, A., Slowik, J. G., Broekhuizen, K., and Abbatt, J. P. D.: Heterogeneous  
555 oxidation of saturated organic aerosols by hydroxyl radicals: uptake kinetics, condensed-phase products,  
556 and particle size change, *Atmos. Chem. Phys.*, 7, 4187-4201, 2007.

557 George, I. J., and Abbatt, J. P. D.: Chemical evolution of secondary organic aerosol from OH-initiated

558 heterogeneous oxidation, *Atmos. Chem. Phys.*, 10, 5551-5563, 2010.

559 Hearn, J. D., and Smith, G. D.: A mixed-phase relative rates technique for measuring aerosol reaction  
560 kinetics, *Geophys. Res. Lett.*, 33, L17805, 10.1029/2006gl026963, 2006.

561 Huisman, A. J., Krieger, U. K., Zuend, A., Marcolli, C., and Peter, T.: Vapor pressures of substituted  
562 polycarboxylic acids are much lower than previously reported, *Atmos. Chem. Phys.*, 13, 6647-6662,  
563 10.5194/acp-13-6647-2013, 2013.

564 Isaacman, G., Chan, A. W. H., Nah, T., Worton, D. R., Ruehl, C. R., Wilson, K. R., and Goldstein, A. H.:  
565 Heterogeneous OH Oxidation of Motor Oil Particles Causes Selective Depletion of Branched and Less  
566 Cyclic Hydrocarbons, *Environ. Sci. Technol.*, 46, 10632-10640, 10.1021/es302768a, 2012.

567 Jacobson, M. Z.: *Fundamentals of Atmospheric Modeling*, Cambridge University Press, 2005.

568 Jayne, J. T., Leard, D. C., Zhang, X., Davidovits, P., Smith, K. A., Kolb, C. E., and R. Worsnop, D.:  
569 Development of an Aerosol Mass Spectrometer for Size and Composition Analysis of Submicron  
570 Particles, *Aerosol Sci. Technol.*, 33, 49-70, 2000.

571 Kessler, S. H., Smith, J. D., Che, D. L., Worsnop, D. R., Wilson, K. R., and Kroll, J. H.: Chemical  
572 Sinks of Organic Aerosol: Kinetics and Products of the Heterogeneous Oxidation of Erythritol and  
573 Levoglucosan, *Environ. Sci. Technol.*, 44, 7005-7010, 10.1021/es101465m, 2010.

574 Kessler, S. H., Nah, T., Daumit, K. E., Smith, J. D., Leone, S. R., Kolb, C. E., Worsnop, D. R., Wilson,  
575 K. R., and Kroll, J. H.: OH-Initiated Heterogeneous Aging of Highly Oxidized Organic Aerosol, *J. Phys.*  
576 *Chem. A*, 116, 6358-6365, 10.1021/jp212131m, 2012.

577 Kolb, C. E., Cox, R. A., Abbatt, J. P. D., Ammann, M., Davis, E. J., Donaldson, D. J., Garrett, B. C.,  
578 George, C., Griffiths, P. T., Hanson, D. R., Kulmala, M., McFiggans, G., P'oschl, U., Riipinen, I., Rossi,  
579 M. J., Rudich, Y., Wagner, P. E., Winkler, P. M., Worsnop, D. R., and Dowd, C. D. O.: An overview of  
580 current issues in the uptake of atmospheric trace gases by aerosols and clouds, *Atmos. Chem. Phys.*, 10,  
581 10561-10605, 2010.

582 Kroll, J. H., and Seinfeld, J. H.: Chemistry of secondary organic aerosol: Formation and evolution of  
583 low-volatility organics in the atmosphere, *Atmos. Environ.*, 42, 3593-3624, 2008.

584 Lambe, A. T., Zhang, J. Y., Sage, A. M., and Donahue, N. M.: Controlled OH radical production via  
585 ozone-alkene reactions for use in aerosol aging studies, *Environ. Sci. Technol.*, 41, 2357-2363,  
586 10.1021/es061878e, 2007.

587 Lambe, A. T., Miracolo, M. A., Hennigan, C. J., Robinson, A. L., and Donahue, N. M.: Effective Rate  
588 Constants and Uptake Coefficients for the Reactions of Organic Molecular Markers (n-Alkanes,  
589 Hopanes, and Steranes) in Motor Oil and Diesel Primary Organic Aerosols with Hydroxyl Radicals,  
590 *Environ. Sci. Technol.*, 43, 8794-8800, 10.1021/es901745h, 2009.

591 Li, P., Al-Abadleh, H. A., and Grassian, V. H.: Measuring heterogeneous uptake coefficients of gases on  
592 solid particle surfaces with a Knudsen Cell reactor: complications due to surface saturation and gas  
593 diffusion into underlying layers., *J. Phys. Chem. A.*, 106, 1210-1219, 2002.

594 Liggio, J., Li, S. M., Vlasenko, A., Sjostedt, S., Chang, R., Shantz, N., Abbatt, J., Slowik, J. G.,  
595 Bottenheim, J. W., Brickell, P. C., Stroud, C., and Leaitch, W. R.: Primary and secondary organic  
596 aerosols in urban air masses intercepted at a rural site, *J. Geophys. Res.-Atmos.*, 115, D21305,  
597 doi:10.1029/2010JD014426., D21305  
598 10.1029/2010jd014426, 2010.

599 Liu, C., Zhang, P., Wang, Y., Yang, B., and Shu, J.: Heterogeneous Reactions of Particulate  
600 Methoxyphenols with NO<sub>3</sub> Radicals: Kinetics, Products, and Mechanisms, *Environ. Sci. Technol.*, 46,  
601 13262-13269, 2012.

602 Liu, Y., Liggio, J., Harner, T., Jantunen, L., Shoeib, M., and Li, S.-M.: Heterogeneous OH initiated  
603 oxidation: A possible explanation for the persistence of organophosphate flame retardants in air,  
604 *Environ. Sci. Technol.*, 48, 1041-1048, 2014.

605 Ma, J., Liu, Y., and He, H.: Degradation kinetics of anthracene by ozone on mineral oxides, *Atmos.*  
606 *Environ.*, 44, 4446-4453, 2010

607 McNeill, V. F., Wolfe, G. M., and Thornton, J. A.: The Oxidation of Oleate in Submicron Aqueous Salt  
608 Aerosols: Evidence of a Surface Process, *J. Phys. Chem. A*, 111, 1073-1083, 2007.

609 McNeill, V. F., Yatavelli, R. L. N., Thornton, J. A., Stipe, C. B., and Landgrebe, O.: Heterogeneous OH  
610 oxidation of palmitic acid in single component and internally mixed aerosol particles: vaporization and  
611 the role of particle phase, *Atmos. Chem. Phys.*, 8, 5465-5476, 10.5194/acp-8-5465-2008, 2008.

612 Norris, G., and Vedantham, R.: EPA positive matrix factorization (PMF) 3.0 fundamentals & user guide,  
613 U.S. Environmental Protection Agency, [www.epa.gov](http://www.epa.gov), 2008.

614 Pöschl, U.: Atmospheric Aerosols: Composition, Transformation, Climate and Health Effects, *Angew.*  
615 *Chem. Int. Ed.*, 44, 7520-7540, 2005.

616 Paatero, P., and Tapper, U.: Positive matrix factorization: a nonnegative factor model with optimal  
617 utilization of error estimates of data values, *Environmetrics* 5, 111-126, 1994.

618 Paatero, P.: Least squares formulation of robust non - negative factor analysis, *Chemom. Intell. Lab.*  
619 *Syst.*, 37, 23-35, doi:10.1016/S0169-7439(96)00044-5., 1997.

620 Paatero, P., and Hopke, P. K.: Discarding or downweighting highnoise variables in factor analytic  
621 models, *Anal. Chim. Acta*, 490, 277-289, 2003.

622 Pankow, J. F.: An absorption-model of gas-particle partitioning of organic compounds in the  
623 atmosphere, *Atmos. Environ.*, 28, 185-188, 1994.

624 Price, H. C., Murray, B. J., Mattsson, J., O'Sullivan, D., Wilson, T. W., Baustian, K. J., and Benning, L.  
625 G.: Quantifying water diffusion in high-viscosity and glassy aqueous solutions using a Raman isotope  
626 tracer method, *Atmos. Chem. Phys.*, 14, 3817-3830, 10.5194/acp-14-3817-2014, 2014.

627 Reff, A., Eberly, S. I., and Bhave, P. V.: Receptor modeling of ambient particulate matter data using  
628 positive matrix factorization: Review of existing methods, *J. Air Waste Manage.*, 57, 146-154, 2007.

629 Renbaum, L. H., and Smith, G. D.: Artifacts in measuring aerosol uptake kinetics: the roles of time,  
630 concentration and adsorption, *Atmos. Chem. Phys.*, 11, 6881-6893, 10.5194/acp-11-6881-2011, 2011.

631 Sareen, N., Moussa, S. G., and McNeill, V. F.: Photochemical Aging of Light-Absorbing Secondary  
632 Organic Aerosol Material, *J. Phys. Chem. A*, 117, 2987-2996, 2013.

633 Schwartz, R. E., Russell, L. M., Sjostedt, S. J., Vlasenko, A., Slowik, J. G., Abbatt, J. P. D., Macdonald,  
634 A. M., Li, S. M., Liggio, J., Toom-Sauntry, D., and Leitch, W. R.: Biogenic oxidized organic  
635 functional groups in aerosol particles from a mountain forest site and their similarities to laboratory  
636 chamber products, *Atmos. Chem. Phys.*, 10, 5075-5088, 10.5194/acp-10-5075-2010, 2010.

637 Slowik, J. G., Wong, J. P. S., and Abbatt, J. P. D.: Real-time, controlled OH-initiated oxidation of  
638 biogenic secondary organic aerosol, *Atmos. Chem. Phys.*, 12, 9775-9790, 10.5194/acp-12-9775-2012,  
639 2012.

640 Smith, J. D., Kroll, J. H., Cappa, C. D., Che, D. L., Liu, C. L., Ahmed, M., Leone, S. R., Worsnop, D.  
641 R., and Wilson, K. R.: The heterogeneous reaction of hydroxyl radicals with sub-micron squalane  
642 particles: a model system for understanding the oxidative aging of ambient aerosols, *Atmos. Chem.*  
643 *Phys.*, 9, 3209-3222, 10.5194/acp-9-3209-2009, 2009.

644 Song, Y., Zhang, Y., Xie, S., Zeng, L., Zheng, M., Salmon, L. G., Shao, M., and Slanina, S.: Source  
645 apportionment of PM<sub>2.5</sub> in Beijing by positive matrix factorization, *Atmos. Environ.*, 40, 1526-1537,

646 2006.

647 Ulbrich, I. M., Canagaratna, M. R., Zhang, Q., Worsnop, D. R., and Jimenez, J. L.: Interpretation of  
648 organic components from Positive Matrix Factorization of aerosol mass spectrometric data, *Atmos.*  
649 *Chem. Phys.*, 9, 2891-2918, 2009.

650 Viana, M., Kuhlbusch, T. A. J., Querol, X., Alastuey, A., Harrison, R. M., Hopke, P. K., Winiwarter, W.,  
651 Vallius, A., Szidat, S., Prevot, A. S. H., Hueglin, C., Bloemen, H., Wahlin, P., Vecchi, R., Miranda, A. I.,  
652 Kasper-Giebl, A., Maenhaut, W., and Hitzenberger, R.: Source apportionment of particulate matter in  
653 Europe: A review of methods and results, *J. Aerosol. Sci.*, 39, 827-849, 10.1016/j.jaerosci.2008.05.007,  
654 2008.

655 Weitkamp, E. A., Hartz, K. E. H., Sage, A. M., Donahue, N. M., and Robinson, A. L.: Laboratory  
656 measurements of the heterogeneous oxidation of condensed-phase organic molecular makers for meat  
657 cooking emissions, *Environ. Sci. Technol.*, 42, 5177-5182, 2008a.

658 Weitkamp, E. A., Lambe, A. T., Donahue, N. M., and Robinson, A. L.: Laboratory Measurements of the  
659 Heterogeneous Oxidation of Condensed-Phase Organic Molecular Makers for Motor Vehicle Exhaust,  
660 *Environ. Sci. Technol.*, 42, 7950-7956, 10.1021/es800745x, 2008b.

661 Widmann, J. F., and Davis, E. J.: Mathematical models of the uptake of ClONO<sub>2</sub> and other gases by  
662 atmospheric aerosols, *J. Aerosol. Sci.*, 28, 87-106, 1997.

663 Wilson, K. R., Smith, J. D., Kessler, S. H., and Kroll, J. H.: The statistical evolution of multiple  
664 generations of oxidation products in the photochemical aging of chemically reduced organic aerosol,  
665 *Phys. Chem. Chem. Phys.*, 14, 1468-1479, 10.1039/c1cp22716e, 2012.

666 Worsnop, D. R., Morris, J. W., Shi, Q., Davidovits, P., and Kolb, C. E.: A chemical kinetic model for  
667 reactive transformations of aerosol particles, *Geophys. Res. Lett.*, 29, 1996, 10.1029/2002gl015542,  
668 2002.

669 Yuan, Z. B., Yu, J. Z., Lau, A. K. H., Louie, P. K. K., and Fung, J. C. H.: Application of positive matrix  
670 factorization in estimating aerosol secondary organic carbon in Hong Kong and its relationship with  
671 secondary sulfate, *Atmos. Chem. Phys.*, 6, 25-34, 10.5194/acp-6-25-2006, 2006.

672 Zhang, Q., Jimenez, J., Canagaratna, M., Ulbrich, I., Ng, N., Worsnop, D., and Sun, Y.: Understanding  
673 atmospheric organic aerosols via factor analysis of aerosol mass spectrometry: a review, *Anal. Bioanal.*  
674 *Chem.*, 401, 3045-3067, 10.1007/s00216-011-5355-y, 2011.

675

676

677

678

679

680

681

682

683

684

685

686

687

688

689

690 **Table 1.** Comparison of the measured  $k_2$  values utilizing PMF and select m/z tracers,  
 691 for organophosphate compounds and CA.

OA	Mean $k_{r\_PMF}$	$k_2 (10^{12}) \text{ cm}^3 \text{ molecule}^{-1} \text{ s}^{-1}$			$k_{2\_PMF}/$ $k_{2\_Tracer}$	$M_{Tracer}/M^+$
		$k_{2, \text{obs\_PMF}}$	$k_{2, \text{t\_PMF}}$	$k_{2, \text{t\_Tracer}}$		
TPhP	1.58±0.33	1.48±0.31	1.95±0.43	2.10±0.19 <sup>a</sup>	0.9	326/326
TDCPP	1.20±0.31	1.13±0.29	1.35±0.35	0.92±0.09 <sup>a</sup>	1.5	381/431
TEHP	3.52±0.65	3.31±0.61	4.25±0.78	2.70±0.63 <sup>a</sup>	1.6	323/435
CA	3.01±0.27	2.83±0.25	3.31±0.29	0.79±0.06	4.2	147/192

692 a.(Liu et al., 2014)

693

694

695

696

697

698

699

700

701

702

703

704

705

706

707

708

709 **Figure captions**

710 **Figure 1.** Changes in (A) total organic mass concentration, (B) the fraction of  
711 unreacted citric acid derived by PMF and (C) products of citric acid oxidized by OH  
712 derived by PMF, as a function of relative experimental time. The values 1 – 6  
713 represent a step-wise O<sub>3</sub> concentration decrease, corresponding to decreased OH  
714 exposure; 0 represents an O<sub>3</sub> concentration of zero. Experimental conditions are  $D_m$ :  
715 200 nm, RH:  $30 \pm 3$  %, T: 298 K.

716 **Figure 2.** Normalized mass spectra of (A) citric acid (PMF factor 1), (B) citric acid  
717 oxidation products (PMF factor 2), and (C) the difference mass spectrum (Factor 2 –  
718 Factor 1). The numbers in the upper two rows are the intensities of m/z 87 and 129,  
719 while negative values are shown in the bottom row. The red and green lines indicate a  
720 negative and positive value, respectively.

721 **Figure 3.** Mass spectra (A) of CA from NIST database, (B) of pure CA measured with  
722 the C-ToF-AMS.

723 **Figure 4.** Comparison between the mass spectra of factor 1 from PMF analysis and  
724 pure CA directly measured by the C-ToF-AMS. The inset graph is the correlation of  
725 their corresponding signal intensities.

726 **Figure 5.** Changes in the relative concentration of (A) methanol, (B) citric acid  
727 extracted with PMF analysis and (C) specific tracers measured with the AMS during  
728 the OH initiated oxidation of citric acid. Experimental conditions are  $D_m$ : 140 nm, RH:  
729  $30 \pm 3$  %, T: 298 K. The values in the top row represent the OH exposures.

730 **Figure 6.** Relative concentration of citric acid ( $c/c_0$ ) as a function of the relative  
731 concentration of methanol based upon (A) PMF analysis, (B) m/z=129 and (C) m/z

732 147. Experimental conditions are  $D_m$ : 140 nm, RH:  $30 \pm 3$  %, T: 298 K.

733

734

735

736

737

738

739

740

741

742

743

744



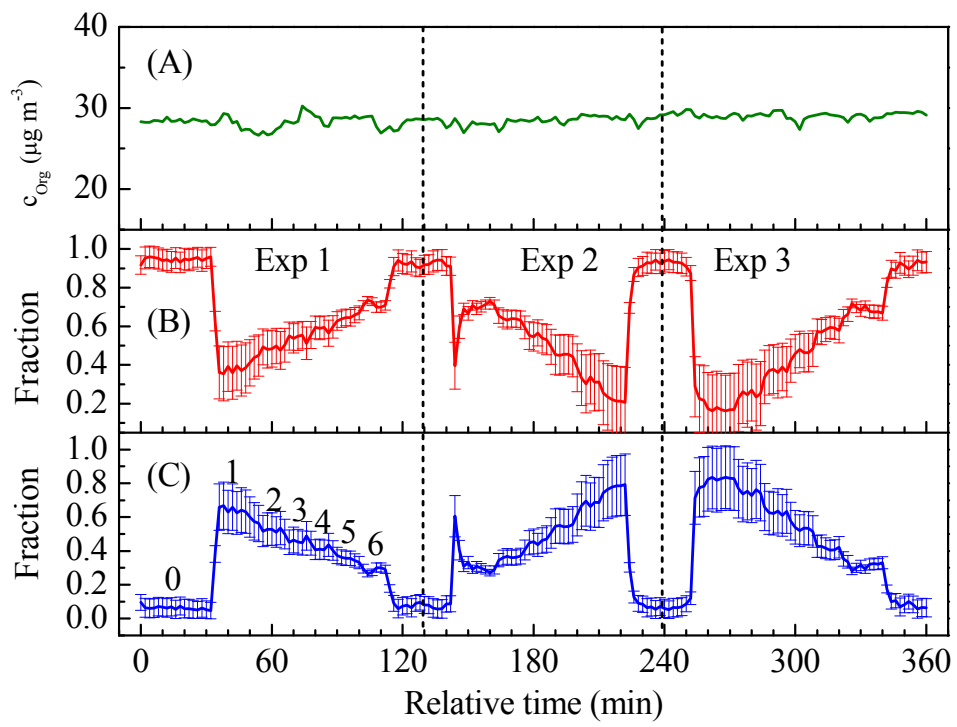


**Figure 1.**

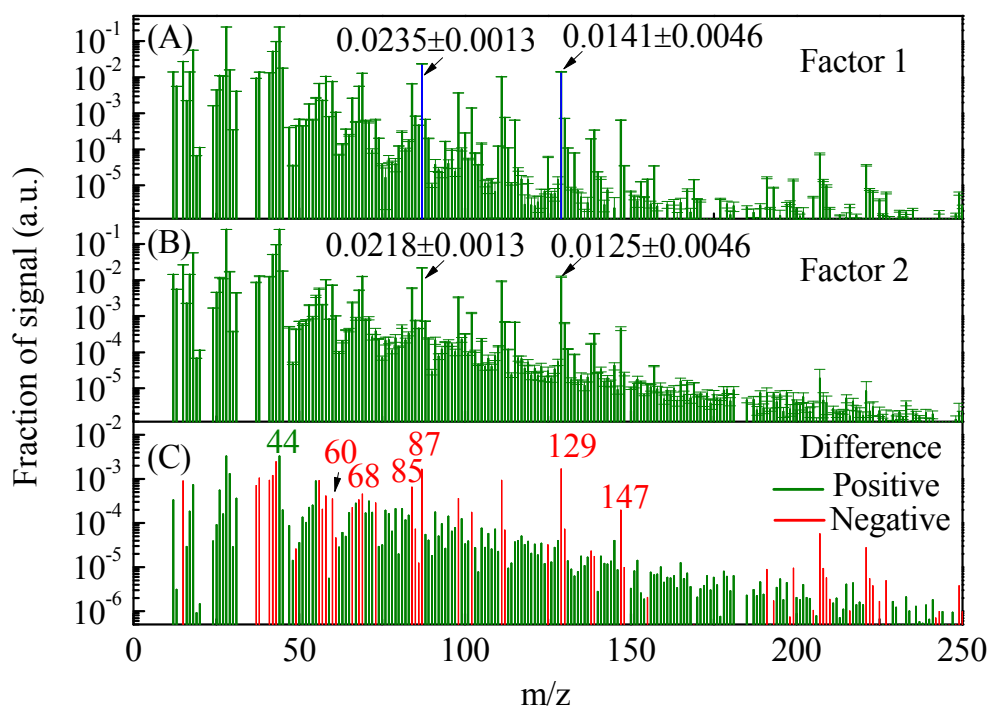
745

746

747

748

749



750

751

752

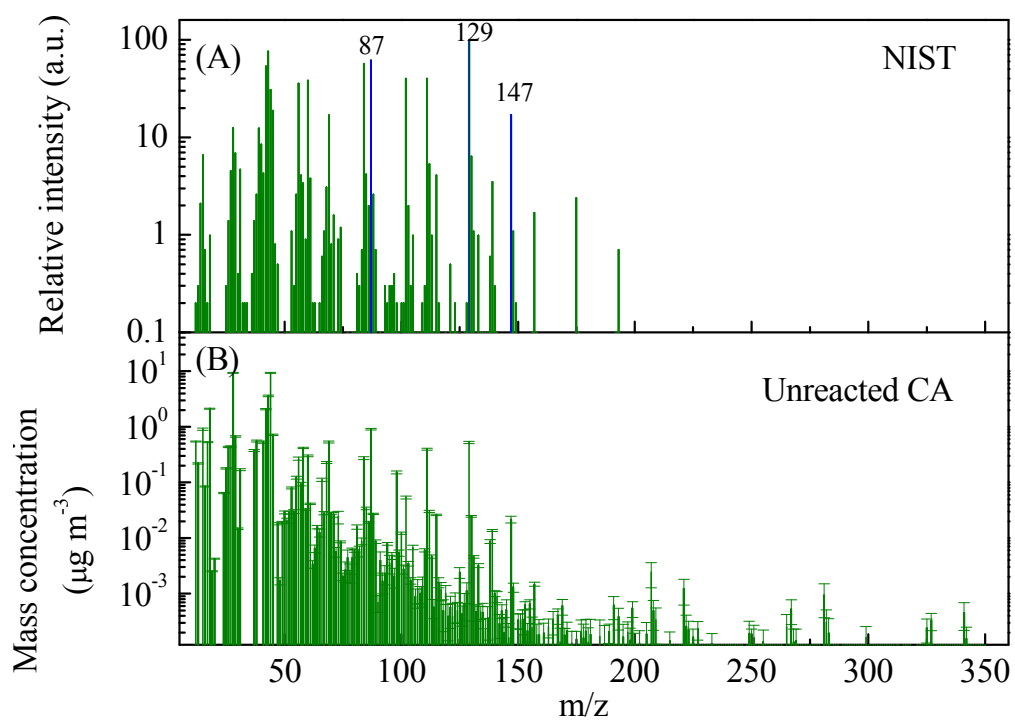
753

754

755

756

**Figure 2.**



757

758

759

760

761

762

763

764

765

766

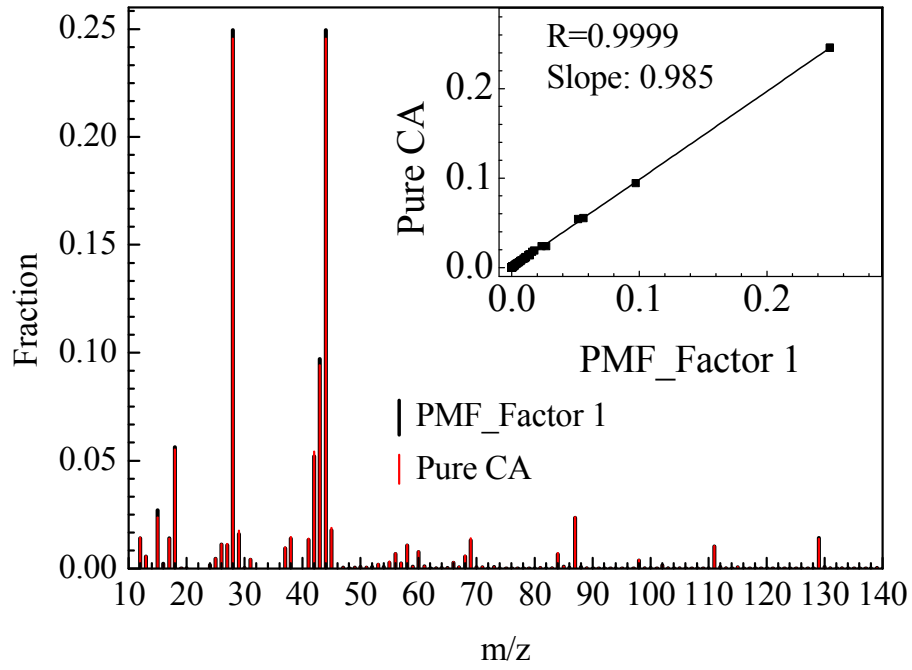
767

768

769

770

**Figure 3.**



771

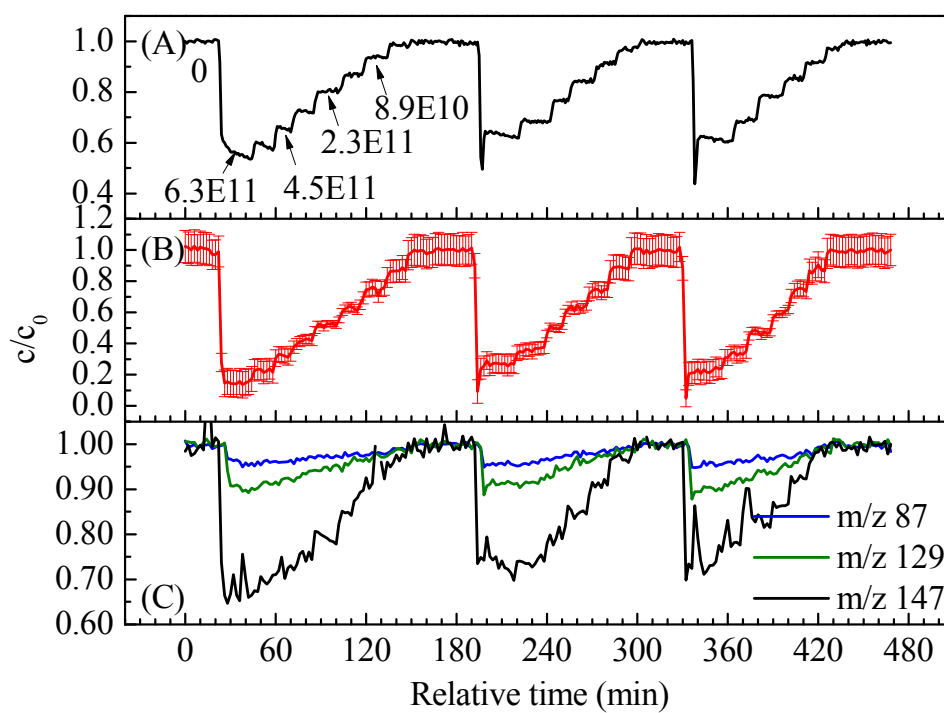
772

773

774

775

**Figure 4.**



776

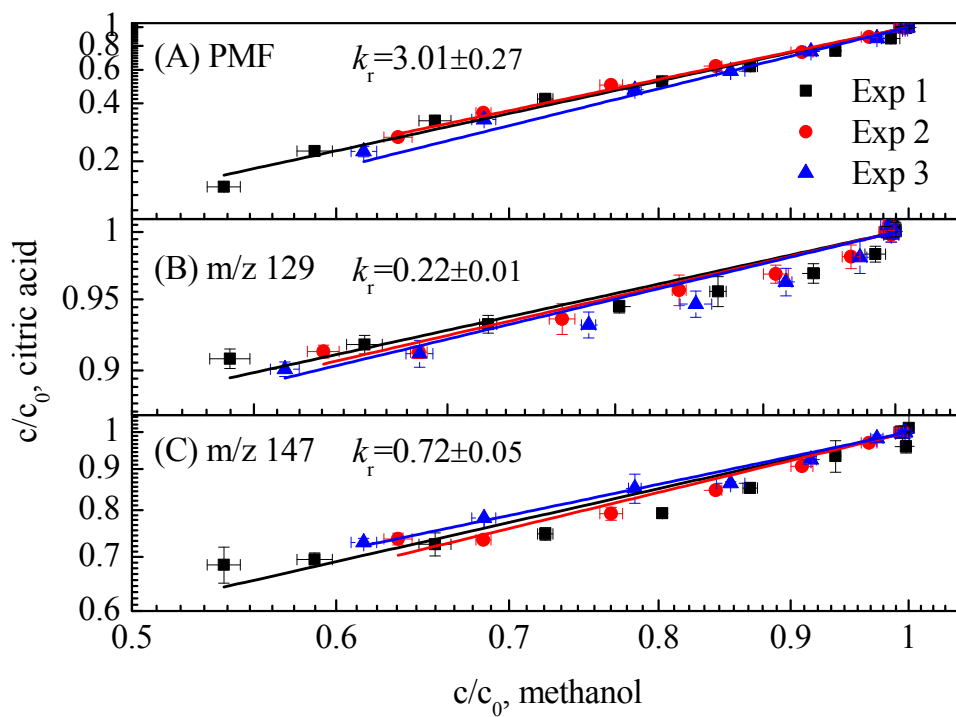
777

778

779

780

**Figure 5.**



781

782

783

**Figure 6.**